HHS Public Access

Author manuscript

Neuron. Author manuscript; available in PMC 2020 September 25.

Published in final edited form as:

Neuron. 2019 September 25; 103(6): 1073–1085.e6. doi:10.1016/j.neuron.2019.07.007.

ADF/Cofilin-Mediated Actin Turnover Promotes Axon Regeneration in the Adult CNS

Andrea Tedeschi[1,2,#], **Sebastian Dupraz**[1,#], **Michele Curcio**[1,3,#], **Claudia J. Laskowski**[1,4,#], **Barbara Schaffran**[1,#], **Kevin C. Flynn**[1,5], **Telma E. Santos**[1], **Sina Stern**[1], **Brett J. Hilton**[1], **Molly J.E. Larson**[2], **Christine B. Gurniak**[6], **Walter Witke**[6], **Frank Bradke**[1,7,*]

[1]Axonal Growth and Regeneration, German Center for Neurodegenerative Diseases (DZNE), Sigmund-Freud-Str. 27, 53127 Bonn, Germany

[2]Present address: Center for Brain and Spinal Cord Repair, Department of Neuroscience, Wexner Medical Center, The Ohio State University, 460 W 12th Ave, Columbus, OH 43210, USA

[3]Present address: VIB Discovery Sciences, Bio-Incubator Leuven, Gaston Geenslaan 1, 3001 Leuven (Heverlee), Belgium

[4]Present address: Klifovet AG, Geyerspergerstr. 27, 80689 Munich, Germany

[5]Present address: Stem Cells, R&D Systems, Inc. 614 McKinley Place NE, Minneapolis, MN 55413, USA

[6]Institute of Genetics, University of Bonn, Karlrobert-Kreiten-Str. 13, 53115 Bonn, Germany

[7]Lead Contact

SUMMARY

Injured axons fail to regenerate in the adult central nervous system, which contrasts their vigorous growth during embryonic development. We explored the potential of re-initiating axon extension after injury by reactivating the molecular mechanisms that drive morphogenetic transformation of neurons during development. Genetic loss- and gain-of-function experiments followed by time-lapse microscopy, *in vivo* imaging and whole-mount analysis show that axon regeneration is fueled by elevated actin turnover. ADF/Cofilin controls actin turnover to sustain axon regeneration after spinal cord injury through its actin-severing activity. This pinpoints ADF/Cofilin as a key regulator of axon growth competence, irrespective of developmental stage. These findings reveal the central role of actin dynamics regulation in this process and elucidate a core mechanism

*Correspondence: Frank.Bradke@dzne.de.
#These authors contributed equally.

AUTHOR CONTRIBUTIONS

C.L., K.F., and F.B. conceived the project; A.T., S.D., M.C., C.L., B.S., and F.B. designed research; A.T., S.D., M.C., C.L., B.S., K.F., T.S., and S.S. performed research; A.T., S.D., M.C., C.L., B.S., K.F., T.S., S.S., M.L., and B.H. analyzed the data; C.G. and W.W. provided mutant mice and antibodies; F.B. supervised the research; A.T.,S.D., M.C., C.L., B.S., and F.B wrote the paper. T.S., S.S., B.J.H., C.G., and W.W. provided feedback and contributed to editing the manuscript.

DECLARATION OF INTERESTS

The authors declare no competing financial interests.

underlying axon growth after CNS trauma. Thereby, neurons maintain the capacity to stimulate developmental programs during adult life, expanding their potential for plasticity. Thus, actin turnover is a key process for future regenerative interventions.

Graphical Abstract

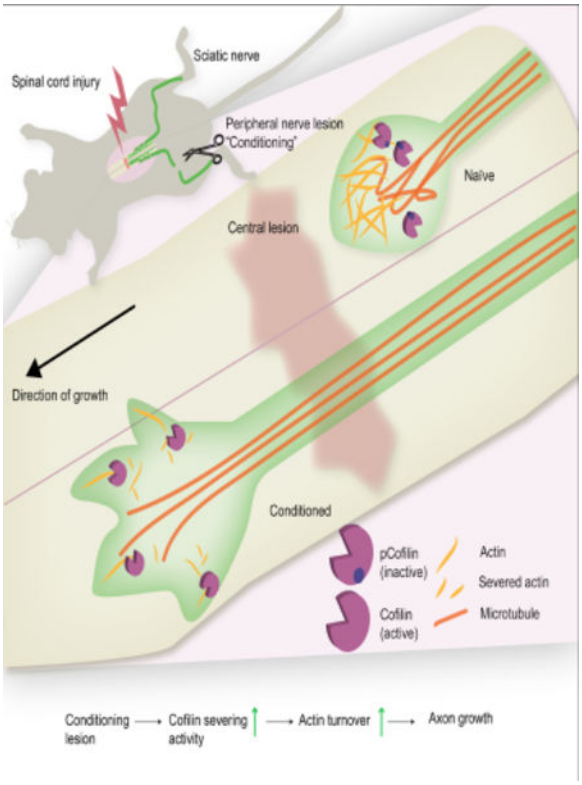

In Brief /eTOC Blurb

Tedeschi et al. identify ADF/Cofilin as a key driver of axon regeneration in adult dorsal root ganglion neurons. Specifically, enhanced actin turnover by the ADF/Cofilin severing function controls axon regeneration in the adult CNS.

Keywords

Axon regeneration; Axon injury; Conditioning; ADF/Cofilin; Actin dynamics

INTRODUCTION

Axons fail to regenerate in the adult mammalian central nervous system (CNS). This limits recovery in neurodegenerative diseases or upon CNS injury (Fawcett, 2015). Regeneration failure is attributed to both extracellular factors that are inhibitory to axon growth (Schwab and Strittmatter, 2014; Silver and Silver, 2014) and the downregulation of neuron-intrinsic regenerative programs (He and Jin, 2016; Tedeschi and Bradke, 2017).

One strategy to induce axon regeneration is to reactivate intracellular processes that drive axon growth during development (Hilton and Bradke, 2017). For example, moderate pharmacological stabilization of microtubules, which elicits axon growth in developing hippocampal neurons (Gomis-Ruth et al., 2008; van Beuningen et al., 2015; Witte et al., 2008), induces axon regeneration after spinal cord injury and leads to functional recovery (Hellal et al., 2011; Ruschel and Bradke, 2017; Ruschel et al., 2015; Sandner et al., 2018). However, the molecular mechanisms and the corresponding evidence of the reactivation of a developmental program have remained fragmentary.

The formation of a growth cone, the ‘sensory and motor organ’ at the tip of growing axons, is critical for axon growth during development and axon regeneration after injury (Bradke et al., 2012; Dent et al., 2011). Actin treadmilling, the assembly of actin filaments at the leading edge of the growth cone and their disassembly at its central domain, regulates growth cone motility (Lowery and Van Vactor, 2009; Rodriguez et al., 2003; Van Goor et al., 2012), neurite formation (Flynn et al., 2012) and axon growth (Bradke and Dotti, 1999; Forscher and Smith, 1988) during development.

Emerging evidence suggests that the actin depolymerizing factor (ADF)/Cofilin (AC) family enhances growth cone dynamics and neurite extension during development by directing actin retrograde flow (Endo et al., 2003; Flynn et al., 2012). AC proteins bind to the aged actin filaments and shorten them by separable severing and depolymerization activities (Bamburg and Wiggan, 2002; Chen et al., 2000; Pollard et al., 2000). Thus, following the concept that axon regeneration can be elicited by reactivating a developmental growth program, AC proteins could be primary candidates to direct axon regeneration in the CNS.

Here we tested the role of actin dynamics in the regeneration of adult rodent dorsal root ganglion (DRG) neurons. These neurons regenerate their central axon when their peripheral axon is lesioned prior to CNS injury, a procedure termed ‘conditioning’ (Neumann and Woolf, 1999; Richardson and Issa, 1984; Tedeschi et al., 2016). While many signaling pathways underlying the conditioning-induced growth have been identified, little is known about the actual physiological processes regulating regenerative growth (Curcio and Bradke, 2018). Our results show that conditioning increases actin dynamics by enhancing the actin-severing activity of AC, which is required for axon regeneration. Thus, AC promotes axon regeneration by recapitulating processes that control neurite extension during development, revealing that adult neurons retain the capacity of activating developmental programs and thereby expanding their potential for plasticity.

RESULTS

Rapid Actin Turnover is Essential for Accelerated Growth After Conditioning

We determined growth cone dynamics of adult conditioned DRG neurons both in cell culture and *in vivo* after spinal cord injury. To condition DRG neurons, we performed unilateral sciatic nerve transection in adult rats. One week later, we dissected the conditioned and contralateral unconditioned (naïve) lumbar (L) 4 and 5 DRGs, and dissociated and plated the neurons to assess growth cone behavior (Figures 1A–D). Time-lapse microscopy showed that axons of cultured conditioned rat DRG neurons, which become long and unbranched

(Figure 1B) (Smith and Skene, 1997), reached a maximum growth rate of 2 μm/minute, and grew in average three times faster than axons of naïve neurons (Figures 1B–1D; Movie S1), which are short and branched (Smith and Skene, 1997). Conditioned growth cones were dynamic, extended long filopodia, and rapidly changed their morphology (Figures S1A–S1D). By contrast, growth cones from naïve DRG neurons contained shorter filopodia and relatively static lamellipodia (Figures S1A–S1D).

Conditioning also enhanced growth cone dynamics *in vivo*. We transected single dorsal column (DC) axons using a localized laser lesion at the L1 level of the spinal cord in naïve or conditioned GFP-M mice as described before (Figure 1E) (Schaffran et al., 2019; Ylera et al., 2009). The dynamics of the proximal stump from injured axons were studied within the first 4.5 h after lesion using two-photon time-lapse microscopy (Figures 1F and 1G). Expectedly, 34% of conditioned axons started growing within this time interval whereas only 12% of naïve axons initiated growth. Notably, the growth cones of conditioned axons generated twice as many protrusions and three times more filopodia than growth cones of naïve axons (Figures 1H and 1I; Movie S2).

To analyze the underlying actin dynamics in the growth cone, we transfected dissociated DRG neurons with the F-actin marker Lifeact fused to green fluorescent protein (GFP) (Riedl et al., 2008) and performed fluorescent time-lapse microscopy. In growth cones from conditioned neurons, actin retrograde flow was increased and actin-based protrusions doubled in frequency, when compared to naïve neurons (Figures 1J–1L; Movie S3).

To determine whether high actin turnover is necessary for rapid axon growth after conditioning, we treated conditioned adult rat DRG neurons with the F-actin stabilizing drug jasplakinolide (Jasp), which suppresses actin dynamics (Figures 2A–2C; Movie S4) (Flynn et al., 2012). Indeed, Jasp treatment inhibited axon extension, mimicking the morphology of naïve neurons (Figures 2D–2F). Thus, accelerated actin turnover is necessary for the rapid axonal growth elicited by a conditioning lesion.

ADF/Cofilin is More Active Following a Conditioning Lesion

Given that AC proteins are critical regulators of actin turnover during neuronal development (Bellenchi et al., 2007; Flynn et al., 2012), we investigated whether the activity of Cofilins, the prevailing AC members, are modulated after a conditioning lesion. Protein extracts from adult conditioned rat L4–5 DRGs showed higher Cofilin activity compared to naïve controls evidenced by reduced phosphorylated Cofilin (pCofilin) (Figures 2G–2I) (Moriyama et al., 1996). Of note, protein levels of the AC family members Cofilin1, Cofilin2 and ADF remained unaltered after conditioning (Figures 2H and 2J–2L). The Cofilin phosphatase Slingshot homolog 1 (SSH1) was also less phosphorylated after conditioning (Figures 2M and 2N), indicating that SSH1 is more active (Figure 2P) (Eiseler et al., 2009), whereas the expression of the upstream kinase that phosphorylates and inactivates Cofilin, LIM kinase (LIMK) (Arber et al., 1998), remained unchanged (Figures 2M, 2O and 2P). Hence, Cofilin is activated after a peripheral nerve lesion and could be involved in conditioning-mediated axon regeneration.

ADF/Cofilin is Required for Conditioning-Mediated Actin Turnover during Axon Regeneration

We tested the physiological role of AC proteins in mediating the conditioning response by assessing the growth of AC Knockout (KO) DRG neurons by using AC knockout (KO) DRG neurons and assessing their growth. To this end, mice deficient in ADF and/or carrying floxed alleles of the Cofilin members were transduced with adeno-associated virus (AAV) expressing enhanced GFP (AAV-eGFP) or Cre recombinase fused to enhanced GFP (AAV-Cre-eGFP), followed by conditioning.

During neuronal development, ADF and Cofilin1 have redundant functions (Bellenchi et al., 2007; Flynn et al., 2012). Furthermore, all three AC family members are expressed in the adult CNS (Gurniak et al., 2014). Consistent with the possibility that their function might also be redundant in adult DRGs, the ablation of single members of the AC family had no effect on axon growth in conditioned neurons (Figure 3). We thus tested the effect of pairwise gene deletion. Ablation of ADF and Cofilin1 (AC1 KO) showed only a moderate reduction in axon growth (Figure 3) and actin dynamics (Figures S2A–S2E; Movie S5). Moreover, conditioned AC1 KO axons regenerated equally as well as conditioned wild-type (WT) axons after a spinal cord injury (Figure S3). Similarly, deletion of either ADF and Cofilin2 (AC2 KO), or Cofilin1 and Cofilin2 (C1C2 KO) moderately affected axon growth and branching (Figure 3). In contrast, the simultaneous depletion of all three AC members in conditioned $ADF^{-/-}Cofilin1^{flox/flox}Cofilin2^{flox/flox}$ mice transduced with AAV-Cre-eGFP (AC1C2 KO, Figure 4A) resulted in a substantial decrease in axon length, increased branching (Figure 3), and a robust reduction in actin turnover compared to WT conditioned neurons (Figures 4B–4D; Movie S6). Thus, AC proteins function redundantly to drive axon elongation in cultured DRG neurons after conditioning.

We therefore tested whether AC proteins are essential for axon regeneration *in vivo* both in the peripheral nervous system (PNS) and in the CNS. To assess PNS regeneration, the L5 DRG of the adult WT or AC1C2 mice was transduced with AAVs for the expression of Cre recombinase and eGFP, followed by a unilateral sciatic nerve crush one week later (Figure S4A). Three days after peripheral nerve lesion, injured axons from mutant AC1C2 KO mice grew less than 1 mm within the sciatic nerve whereas WT axons grew more than 4 mm (Figure S4). Hence, axon regeneration in the PNS requires AC activity.

Importantly, axon regeneration after central injury also depended on AC proteins. In the spinal cord, four weeks after a dorsal column injury at thoracic (T) 12 level, we visualized regenerating axons of WT and AC1C2 KO conditioned DRG neurons by two photon imaging of whole mount spinal cord samples (Hilton et al., 2019; Tedeschi et al., 2016). As expected, conditioned WT axons regenerated across the injury site. In contrast, conditioned AC1C2 KO axons stalled caudal to the lesion, similar to axons of sham lesioned WT animals (Figures 4E–4G). Thus, AC proteins are critical for driving the regenerative response in peripheral and central axons.

The Severing Activity of Cofilin1 is Essential for Axon Regeneration

To assess which function of AC drives axon regeneration, we reintroduced into AC1C2 KO neurons wildtype Cofilin1(WT) or Cofilin1 mutants that either exclusively sever or depolymerize actin filaments (Moriyama and Yahara, 1999, 2002) (Figure 5A). All of the mutant forms were inserted in the same plasmid backbone, packaged in the same AAV capsid and displayed similar expression levels (Figure S5A and S5B). In cultured conditioned AC1C2 KO neurons, expression of mutant Cofilin1(S94D) fused to red fluorescent protein (RFP), which depolymerizes but does not sever actin filaments (Figure 5A) (Moriyama and Yahara, 1999, 2002), failed to restore actin dynamics (Figures 5B–5D; Movie S7) and axon growth (Figures 5E–5G). By contrast, the expression of the mutant Cofilin1(Y82F), which severs but does not depolymerize actin filaments (Figure 5A) (Moriyama and Yahara, 1999, 2002), restored actin turnover (Figures 5B–5D; Movie S7) and axon growth, albeit to a lesser extent than expression of Cofilin1(WT) (Figures 5E–5G). We also tested Cofilin1 (S3A), a non-phosphorylatable form of Cofilin1. Phosphorylation on Serine at position 3 (S3) not only determines Cofilin deactivation but also its turnover from actin-bound to actin-free state (Pak et al., 2008). Therefore in developing neurons, overexpression of non-phosphorylatable Cofilin1(S3A) induces a similar enhancement in axon growth compared to Cofilin(WT) (Endo et al., 2003). Consistently, overexpression of a Cofilin1(S3A) mutant in cultured AC1C2 KO adult naïve neurons showed a comparable rescue of axon extension as overexpression of Cofilin1(WT) (Figures S5C and S5D). We next tested whether the severing activity of Cofilin1 is critical for axon regeneration *in vivo*. The sciatic nerve of adult AC1C2 mice was transduced with AAVs expressing Cre, eGFP and one of the Cofilin1 mutants described above (Figure 6A). One week after conditioning, the spinal cord was injured at T12 level and regeneration of centrally projecting DRG axons was evaluated 4 weeks later. We found that expression of the Cofilin1(Y82F) mutant but not of the Cofilin1(S94D) mutant restores regeneration in conditioned AC1C2 KO axons comparably to the effects of Cofilin1(WT) expression (Figures 6B and 6C). Thus, the actin-severing function of Cofilin1 mediates actin turnover and axon regeneration upon conditioning.

Cofilin1 Induces Axon Regeneration

Conditioning triggers various molecular events that ultimately lead to substantial axon regeneration (He and Jin, 2016). We asked whether AC overexpression alone would be sufficient to induce a regenerative response without prior conditioning. As AC proteins compensate for each other, we focused our experiments on Cofilin1, the ubiquitously expressed AC-member. In cell culture, naïve rat neurons overexpressing Cofilin1(WT) extended longer axons when plated on the growth promoting substrate laminin (Figures 7A and 7B) or on the inhibitory substrates chondroitin sulfate proteoglycans (CSPGs) (Silver and Silver, 2014) (Figures 7C and 7D) and Nogo-A (Schwab and Strittmatter, 2014) (Figures 7E and 7F). Based on these findings, we tested whether Cofilin1 overexpression could promote axon regeneration in the adult CNS without a prior conditioning lesion. In adult naïve WT mice, the sciatic nerve was injected with AAV-Cofilin1(WT) in combination with AAV-eGFP to trace regenerating DC axons, followed by a spinal cord injury at T12 level two weeks later (Figure 7G). Four weeks after injury, we found that naïve axons expressing Cofilin1(WT) successfully regenerate and cross the injury site (Figures 7H and 7I; Movie

S8). Overexpression of Cofilin1(S3A) and Cofilin1(Y82F) also evoked a regenerative response, while overexpression of the Cofilin1(S94D) mutant failed to induce axon regeneration (Figures S6B and S6C). In conclusion, Cofilin1 drives axon regeneration in the adult rodent CNS through its actin-severing activity.

DISCUSSION

In this study, we identified ADF/Cofilin-mediated actin turnover as a molecular effector mechanism to induce axon regeneration, by recapitulating processes that elicit neurite growth during development. Our findings highlight the dormant potential in the adult CNS to reactivate developmental programs to expand its plasticity.

Actin Dynamics as a Regulator of Axon Regeneration

During development, a neuron undergoes a rapid series of morphogenetic changes, transforming from a spherical cell into one bearing an axon and dendrites (Dotti et al., 1988; Takano et al., 2015; Yogev and Shen, 2017). One early step in this transformation is the generation of neurites tipped with a highly dynamic growth cone (Flynn et al., 2012; Yogev and Shen, 2017). The growth cone probes the cellular environment to guide the axon to its target. Upon arrival, the growth cone reduces its dynamics and transforms into a *presynaptic* terminal. This is likely mediated by changes in the actin network. Whereas actin filaments in growth cones are dynamic to drive growth cone motility and thereby axon growth (Bradke and Dotti, 1999; Dent et al., 2011; Endo et al., 2003; O'Connor and Bentley, 1993), actin filaments have relatively little turnover in mature axons integrated in circuits (Coles and Bradke, 2015). Are enhanced actin dynamics sufficient to reactivate an axon growth program in adult neurons (Blanquie and Bradke, 2018)? Our time-lapse *in vivo* analysis combined with cell culture imaging and pharmacological experiments revealed that increased actin turnover underlying enhanced growth cone dynamics is critical for regenerative conditioned growth. Adult DRG neurons grow slowly and display the arborizing pattern typically found during synaptogenesis (Smith and Skene, 1997; Tedeschi et al., 2016); however, after conditioning, they show the enhanced actin dynamics necessary for the elongating growth of developing neurons. This suggests that reactivating actin dynamics transforms adult neurons back into an active growth state to elicit axon regeneration. We will discuss next how this reactivation of actin dynamics is mediated.

ADF/Cofilin is Necessary and Sufficient for Axon Regeneration

In isolation, actin filaments are stable polymers with spontaneous depolymerization that is too slow to maintain the fast actin dynamics observed in living cells. Therefore, neurons need accessory proteins to trigger a fast disassembly of aging actin networks (Brieher, 2013; Coles and Bradke, 2015; Ono, 2007). AC is a well-known regulator of actin dynamics, highly expressed in growth cones, and plays a vital role in growth cone motility and axon growth during development (Bamburg and Bray, 1987; Endo et al., 2003; Flynn et al., 2012; Garvalov et al., 2007; Kuhn et al., 2000; Meberg, 2000; Sivadasan et al., 2016), which makes AC a well-suited candidate to control regenerative growth. Upon AC inactivation, the actin network may be static while reactivation of AC could lead to growth competence. Here, we show that AC is activated upon conditioning. This activation of AC proteins is

essential for regeneration of conditioned axons as our genetic ablation analysis combined with time-lapse experiments and *in vivo* studies, revealed that complete loss of AC activity in conditioned neurons abrogates both actin dynamics and axon regeneration.

The genetic analysis was challenged by the expression of a third member of the AC family in the adult nervous system, Cofilin2, which can compensate for the loss of ADF and Cofilin1, but is not expressed in the embryonic nervous system (Gurniak et al., 2014; Gurniak et al., 2005; Kremneva et al., 2014; Vartiainen et al., 2002). While the exact biochemical differences among the isoforms are still controversial, all three members of the AC family have F-actin binding, severing, and depolymerizing activities (Bamburg and Bernstein, 2010; Kremneva et al., 2014; Vartiainen et al., 2002). The combinatorial ablations of two AC members showed very little difference in their axon growth patterns, implying that the three isoforms have redundant functions.

Noteworthy, AC is not only necessary for regenerative growth but overexpression of Cofilin1 without prior conditioning was also sufficient to induce regeneration, both in cell culture as well as *in vivo* after spinal cord injury. While gene transcription and production of cellular material necessary for extensive growth are involved in a full regenerative response triggered by conditioning (He and Jin, 2016), AC-mediated actin turnover turns out to be a key regulator of regenerative growth.

Conditioning-mediated Regeneration - From Transcriptional Changes to Cytoskeletal Effects

The conditioning lesion is the classical regenerative paradigm with arguably the most robust and strongest effect on axon regeneration. Pioneering studies performed decades ago (McQuarrie et al., 1977; Richardson and Issa, 1984) triggered an immense research effort to dissect the associated transcriptional changes (Chandran et al., 2016; Cho et al., 2015; Costigan et al., 2002; Hu et al., 2016; Oh et al., 2018; Puttagunta et al., 2014; Tedeschi et al., 2016; Weng et al., 2018). These efforts revealed numerous pro-regenerative transcription factors, including activating transcription factor (*Atf3*) and signal transducer and activator of transcription (*Stat3*), regenerative associated genes, including growth associated protein 43 (*GAP43*) and small proline rich protein 1 (*Sprr1a*) (Chandran et al., 2016; Cho et al., 2015; Costigan et al., 2002; Tedeschi, 2011), as well as growth suppressors, such as *Cacna2d2* (Tedeschi et al., 2016). By focusing on fundamental cell biological processes that drive neurite and axon growth during development, our work used a complementary approach to help decipher the conditioning response.

Cell biological analysis combined with *in vivo* molecular manipulation identified the severing function of AC as a key molecular process to drive conditioning-mediated axon regeneration. Focusing on the effector mechanisms, we present a novel perspective of how neurons regenerate, by rendering the actin cytoskeleton dynamic and recapitulating molecular processes that drive neurite growth. It is tempting to speculate how actin-manipulating drugs, including cytochalasins and latrunculins, could stimulate axon regeneration as they have proven to stimulate axon elongation in developing neurons (Bradke and Dotti, 1999, 2000; Conde et al., 2010; Kunda et al., 2001). Future pharmacological actin manipulations need to be well-adjusted so that non-neuronal cells at

the lesion site are able to preserve their essential actin-based elements, including tight junctions. Upstream signaling events mediating the observed dephosphorylation of the Cofilin phosphatase SSH1 could include various pathways (reviewed in Mizuno, 2013) involving the phosphatase calcineurin (Wang et al., 2005), protein serine/threonine phosphatases (Oleinik et al., 2010), cyclic AMP signaling (Meberg et al., 1998; Neumann et al., 2002; Qiu et al., 2002), protein kinase D1 (PKD1), 14–3-3 proteins (Eiseler et al., 2009; Kaplan et al., 2017), and phosphatidylinositol 3-kinase (PI3K) (Nishita et al., 2004). Understanding how the reported conditioning-mediated transcriptional changes act upstream of SSH1 and AC activity will be an important direction for future investigations.

CONCLUSION

Current attempts to reactivate the intrinsic growth program to induce axon regeneration focuses on the manipulation of global upstream signaling cascades (Cho et al., 2013; Sun et al., 2011; Tedeschi and Bradke, 2017; Tedeschi et al., 2016). These manipulations change the regenerative state through largely undefined downstream effectors. Here, we show that a single family of actin-regulating proteins, which controls movement and motility in cellular processes as diverse as locomotion and invasive protrusion of tumor cells (Bravo-Cordero et al., 2013), fibroblast migration (Dawe et al., 2003), Listeria motility (Rosenblatt et al., 1997), and tip growth in plants (Augustine et al., 2008), acts as a crucial regulator of axon regeneration. By recapitulating cytoskeletal changes found in newly born nerve cells that break their symmetry to form neurites (Flynn et al., 2012), injured neurons switch to a regenerative state. Thus, AC acts as central regulator of neuronal growth competence, dictating the regenerative fate. This implies activation of AC in injured CNS axons as a promising strategy for future regenerative therapies.

STAR METHODS

LEAD CONTACT AND MATERIALS AVAILABILITY

This study did not generate new unique reagents. Further information and requests for resources and reagents should be directed to and will be fulfilled by the Lead Contact Frank Bradke (Frank.Bradke@dzne.de).

EXPERIMENTAL MODEL AND SUBJECT DETAILS

Animals—All animal experiments were performed in accordance with the Animal Welfare Act and the guidelines of the Landesamt für Natur, Umwelt und Verbraucherschutz (LANUV). Adult female Sprague Dawley rats (RjHan:SD, 175–199 g, Janvier Labs), wild type (WT, C57BL/6J, Charles River) and transgenic mice of both genders (7–8 weeks old) were used as indicated. Thy1-GFP line M (GFP-M, Stock No: 007788) and the Cre reporter strain B6.Cg-Gt(ROSA)26Sor$^{tm9(CAG\text{-}tdTomato)Hze}$/J (Stock No: 007909) were purchased from the Jackson laboratories. ADF$^{-/-}$, Cofilin1$^{flox/flox}$ and Cofilin2$^{flox/flox}$ models have been previously described (Bellenchi et al., 2007; Gurniak et al., 2014; Gurniak et al., 2005). Generation of ADF$^{-/-}$Cofilin1$^{flox/flox}$, ADF$^{-/-}$Cofilin2$^{flox/flox}$, Cofilin1$^{flox/flox}$Cofilin2$^{flox/flox}$, ADF$^{-/-}$Cofilin1$^{flox/flox}$Cofilin2$^{flox/flox}$ was achieved by crossing the appropriate mouse lines. Ablation of AC proteins in the DRG neurons was

achieved by injecting mice with AAV expressing Cre recombinase alone (AAV-Cre) or Cre fused to eGFP (AAV-Cre-eGFP) into the sciatic nerve or directly into the L5 DRG. For SCI regeneration and actin dynamics experiments, $ADF^{-/-}Cofilin1^{flox/flox}$ mice were crossed with the B6.Cg-Gt(ROSA)26Sor$^{tm9(CAG-tdTomato)Hze}$/J line and the CAG promoter-driven red fluorescent protein variant tdTomato was expressed following Cre-mediated recombination. In this set of experiments, $ADF^{+/+}Cofilin1^{+/+}$B6.Cg-Gt(ROSA)26Sor$^{tm9(CAG-tdTomato)Hze}$/J mice were used as controls.

METHOD DETAILS

Conditioning paradigm—Mice and rats were anesthetized with a mixture of ketamine (100 mg/kg body weight) and xylazine (10 mg/kg body weight). The left sciatic nerve was exposed at the mid-thigh level, ligated and cut distally to the ligation site. Naïve or sham operated animals were used as controls for *in vitro* and *in vivo* experiments respectively, as indicated in the text. Animals were allowed to recover for 7–14 days before dissecting L4–5 DRGs or before SCI, as indicated in the text.

DRG culture—Primary DRG neurons from adult naïve and conditioned rats or mice were dissected, dissociated and cultured as previously described (Neumann et al., 2002). In brief, L4–5 DRGs were dissected, collected and rinsed in ice-cold Hank's balanced salt solution (HBSS, Thermo Fisher, 14025–100) supplemented with 7 mM HEPES (Thermo Fisher, 15630–056). After removing the surrounding connective tissue, the ganglia were transferred into a sterile tube, and incubated in collagenase type I (3000 U/ml, Worthington, LS004196) for 45 min (mouse DRGs) or 80 min (rat DRGs) at 36.5 °C, washed once with HBSS, followed by 15 min with Trypsin (0.25%, Thermo Fisher, 25200–056) at 36.5 °C. Enzymatic digestion was stopped by addition of complete Neurobasal-A medium (NB, Thermo Fisher, 12349–015) containing 5% horse serum (PAN biotech, P300702). Neurons were then recovered by centrifugation at 630 rpm for 5 min and gently resuspended in complete NB medium. In some experiments, dissociated neurons were electroporated with plasmid DNA (1 μg per dissected ganglion) by using the appropriate electroporation buffer with Amaxa Nucleofector system (program G-013, Lonza). Dissociated neurons were cultured at low density on dishes or coverslips coated with poly-L-lysine (1 mg/ml in borate buffer, SigmaAldrich, P2636) and laminin (5 μg/ml in water, Roche, 11243217001) and incubated at 36.5 °C in a humidified atmosphere con taining 5% CO_2 for the indicated times. For live-cell imaging, neurons were grown on 35 mm glassbottom dishes (MatTek, P35G-1.5–14-C or P35G-1.5–20-C). For immunocytochemistry, cells were cultured on 13 mm glass coverslips (Marienfeld, #01–115 30) contained in 4-well dishes (Thermo Fisher, 179820). For actin dynamics studies, dissociated rat or mouse DRG neurons were electroporated with Lifeact-GFP plasmid DNA (Riedl et al., 2008). For overexpression experiments, dissociated rat DRG neurons were electroporated with RFP (referred to as "Ctr"), Cofilin1(WT)-RFP, Cofilin1(S94D)-RFP, Cofilin1(Y82F)-RFP expressing plasmid DNA. The electroporation medium was replaced with fresh medium 2 h after plating. For drug treatment, Jasplakinolide (Jasp, 2.5–10 nM, Biomol, Cay11705) or DMSO (0.2%, Sigma-Aldrich, D5879) were added to the culture medium 2 h after plating. For gain-of-function experiments, coverslips were coated with chondroitin sulfate proteoglycans (CSPGs; 0.9–1

μg/ml, Merck Millipore, CC117); in other experiments, cells were cultured in complete NB complemented with laminin (5 μg/ml) and Nogo-A (500 ng/ml, R&D Systems, 3728-NG).

Immunocytochemistry—Prior to fixation, DRG neurons were rinsed once with pre-warmed phosphate buffered saline (PBS, Applichem, A0965,9050). Neurons were fixed with 4% paraformaldehyde (Merck Millipore, 104005) and 4% sucrose (Fluka, 84100) for 15 min. Subsequently, free aldehyde groups were quenched with 50 mM ammonium chloride in PBS and the cells were washed repeatedly with PBS. After permeabilization with 0.1% Triton X-100 (Sigma-Aldrich, X100–100ML) for 5 min, cells were washed again with PBS. Coverslips were then blocked with blocking solution (2% fetal bovine serum, 2% bovine serum albumin and 0.2% fish gelatin in PBS) at room temperature (RT) for 30 min. Coverslips were subsequently incubated with mouse anti-tubulin beta 3 antibody (1:1000, Tuj1, Biolegend, #801201) at RT for 1–2 h. After several rinses in PBS, the coverslips were incubated with the appropriate Alexa Fluor conjugated secondary antibodies (1:500, Invitrogen) and washed in PBS before mounting onto microscope slides. Images were randomly taken with an Axiovert or Axio Observer D1 microscope (Zeiss) and analyzed using ImageJ analysis software (NIH, USA). The average length per condition was calculated by imaging and measuring the longest neurite of each cell. For quantification of the branching frequency, all primary branches were counted along the longest axon and expressed as number of branching points/100 μm. This was carried out in at least three independent experiments. The number of neurons for each condition is indicated in the corresponding figure legend.

Live-cell microscopy

Growth cone dynamics: A heating system (Ibidi) combined with an active gas mixer (Live Imaging Services) for live-cell imaging and video microscopy was used to image neurons under optimal conditions for growth (36.5 °C and 5% CO_2). Living cells were kept on the stage of a fluorescence microscope (Axio Observer D1; Zeiss) in dishes filled with complete NB medium without phenol red. A Plan-Apochromat 100x NA 1.4 objective (Zeiss) was used. Cells were illuminated with the Illuminator HXP 120 C (Zeiss). Halogen light was set to minimal intensity to avoid phototoxicity. Images were captured using a CCD camera (AxioCam MRm, Zeiss). Pictures were recorded using AxioVision microscope software (Zeiss). Growth rate was measured using ImageJ analysis software. The rate of advance of individual growth cones was measured every minute over a time period of 1 h. Growth cone dynamics were quantified over a time period of 2 min by measuring changes of growth cone area every 10 s. Growth cones were outlined manually using MetaMorph Microscopy Automation and Image Analysis Software (Molecular Devices). Growth cone outlines were pasted onto the following images and changes of growth cone area between single images were added together to calculate a total growth cone area change over time. Length of membrane protrusions was measured using ImageJ analysis software.

Actin dynamics: Imaging was performed using a 60x NA 1.6 objective (Olympus) on a DeltaVision RT (GE Healthcare Life Sciences) live-cell imaging setup based on an Olympus IX71 inverted microscope, with a CO_2 regulated incubation chamber maintained at 36 °C (Solent Scientific). Im ages were acquired for 5 min at 3 s intervals with a Photometrics

CoolSnap HQ camera (Roper Scientific) using SoftWoRx 3.5.0 imaging software (Applied Precision). The analysis of various parameters for actin dynamics was performed using MetaMorph imaging software. Linescans around the perimeter of growth cones were used to measure actin retrograde flow and protrusion frequency. Retrograde flow was measured as the slope of diagonal lines in kymographs that were acquired by using MetaMorph software (Flynn et al., 2012). For protrusion frequency, all protrusions ≥ 1 μm were counted.

In vivo* imaging and laser lesion—In vivo* imaging and laser lesions were performed as described previously (Schaffran et al., 2019; Ylera et al., 2009). Briefly, adult female transgenic mice expressing GFP under the control of Thy1 promoter line M (Feng et al., 2000) were conditioned 1 week before *in vivo* imaging. Imaging and lesions were performed with a two-photon Zeiss LSM7MP microscope equipped with an Insight X3 laser and a 40 x NA 1.0 objective (Zeiss). Fluorescence emission was filtered by a dichroic mirror (LP555) and a bandpass filter (BP 500–550), detecting the GFP signal with a non-descanned detector (NDD).

On the day of lesion and imaging mice were anesthetized with a mixture of ketamine (100 mg/kg body weight) and xylazine (10 mg/kg body weight). An L1 laminectomy was performed and the spinal cord was clamped at the adjacent vertebrae with an STS-A spinal cord holder (Narishige). The site of the laminectomy was covered with silicone elastomer (Kwik Sil, World Precision Instruments) and a 5 mm, round cover glass (Harvard Apparatus). The lesions were done with a 40x water immersion objective at 920 nm at maximum power of 130 mW for 2 – 4 s and a pixel dwell time of 121.02 μs. Images were acquired every 2 min from the time of lesion of lesion up to 4.5 hours post-lesion. Imaging was stopped to adjust the focus or field of view, applying water as an immersion, or to supplement with additional anesthesia. After the imaging session mice were transcardially perfused with PBS and ice-cold 4% PFA. The spinal cord and DRGs were dissected and axons were confirmed to arise from DRGs L4–5. Analysis was conducted on maximum intensity projections of z-stacks spaced by 1 μm. Images were filtered with a median filter in ImageJ analysis software.

Protrusion frequency: Protrusions were counted from kymographs over timelapse series every 2 min in dynamic areas of the axons for 30 min to 1 hour, around 2–4 hours post lesion.

Filopodia frequency: Filopodia-like structures were counted manually after lesions for all images acquired within 4.5 hours.

AAV-transduction—Mice were anesthetized with a mixture of ketamine (100 mg/kg body weight) and xylazine (10 mg/kg body weight). Approximately 2 μl of AAV1 particles (>$4e^{12}$ genome copies (GC)/ml, UPenn Vector Core Facility) were injected into the sciatic nerve using a Hamilton syringe connected to a pulled glass micropipette. After 14 days, DRGs were dissected or animals subjected to further surgeries (e.g. conditioning lesion, sciatic nerve crush or SCI). The following commercially available AAVs were used: AAV1.CMV.PI.Cre.rBG (AAV-Cre, AV-1-PV1090), AAV1.CMV.HI.eGFP-Cre.WPRE.SV40 (AAV-Cre-eGFP, AV-1-PV2004) and AAV1.CMV.PI.eGFP.WPRE.bGH (AAV-eGFP, AV-1-

PV0101). The following custom-made (UPenn Vector Core, Philadelphia) AAVs were used: AAV1.CMV.PI.RFP.WPRE.bGH, AAV1.CMV.PI.hCofWT-RFP.WPRE.bGH, AAV1.CMV.PI.hCofS3A-RFP.WPRE.bGH AAV1.CMV.PI.hCofY82F-RFP.WPRE.bGH and AAV1.CMV.PI.hCofS94D-RFP.WPRE.bGH which were referred to as AAV-RFP "AAV-Ctr", AAV-Cof1(WT), AAV-Cof1(S3A), AAV-Cofi1(Y82F) and AAV-Cof1(S94D) respectively. For *in vitro* studies (evaluation of axon length or actin dynamics), the left sciatic nerve of $ADF^{-/-}$ mice was injected with AAV-eGFP, while the left sciatic nerve of $Cofilin1^{flox/flox}$, $Cofilin2^{flox/flox}$, $ADF^{-/-}Cofilin1^{flox/flox}$, $ADF^{-/-}Cofilin2f^{flox/flox}$, $Cofilin1^{flox/flox}Cofilin2^{flox/flox}$ and $ADF^{-/-}Cofilin1^{flox/flox}Cofilin2^{flox/flox}$ mice was injected with AAV-Cre-eGFP. For the CNS regeneration experiments, dorsal column (DC) axons were traced by injecting AAV-Cre into the left sciatic nerve of $ADF^{-/-}Cofilin1^{flox/flox}tdTomato^{flox/flox}$ (AC1 KO) mice or by co-injecting AAV-Cre and AAV-eGFP (1:1 mixture) into $ADF^{-/-}Cofilin1^{flox/flox}Cofilin2^{flox/flox}$ (AC1C2 KO). The rescue experiments of *in vivo* axon regeneration in AC1C2 KO animals were performed by co-injecting into the left sciatic nerve of AC1C2 animals AAV-Cre, AAV-eGFP and one of the following AAVs: AAV-Ctr, AAV-Cofilin1(WT)-RFP, AAV-Cofilin1(Y82F)-RFP or AAV-Cofilin1(S94D)-RFP. For PNS regeneration AAV-Cre and AAV-eGFP (1:1 mixture) were injected into the left L5 DRG of WT and AC1C2 mice. For the rescue experiments *in vitro*, the sciatic nerve of AC1C2 animals was injected with a 1:1 mixture of AAV-Cre-eGFP and AAV-Cofilin1(WT)-RFP, AAV-Cofilin1(Y82F)-RFP or AAV-Cofilin1(S94D)-RFP, respectively. For the overexpression experiments, the sciatic nerve of naïve WT mice was injected with a 1:1 mixture of AAV-eGFP and AAV-Ctr or AAV-Cofilin1(WT)-RFP, respectively.

Spinal cord injury—Mice were anesthetized with an intraperitoneal injection of ketamine (100 mg/kg body weight) and xylazine (10 mg/kg body weight) mixture. SCI was performed as previously described (Tedeschi et al., 2016). Briefly, a T11-T12 laminectomy was performed and the spinal cord was crushed with modified #5 forceps (Dumont, FST) to sever DC axons completely. Mice were transcardially perfused with 4% paraformaldehyde one to four weeks following SCI. The spinal cord was then dissected and post-fixed in 4% paraformaldehyde overnight and then transferred to 30% sucrose in 0.1 M PBS. Imaging of the unsectioned spinal cord was performed using a 2-photon microscope (LSM 7MP, Zeiss). The presence of infiltrating macrophages containing autofluorescent phagocytic material was used to accurately locate the lesion epicenter. Quantification of DC axon regeneration was performed as previously described (Tedeschi et al., 2016). Briefly, the number of regenerating axons at different distances from the lesion epicenter was normalized to the number of labeled axons caudal (200–400 μm) to the lesion. The completeness of the lesion and tracing efficiency were confirmed using transverse sections of the spinal cord (3 mm caudal and 7–8 mm rostral to the lesion). Mice with incomplete lesions were excluded from further analysis. In a set of experiments, quantification of axon regeneration *in vivo* was performed on sagittal sections of the spinal cord following standard protocols (see also immunohistochemistry section). In these samples, the lesion epicenter was identified by axon morphology and glial fibrillary acidic protein (GFAP) staining. Videos of 3D rendered dorsal column sensory axons were constructed using the Imaris Animation function.

Immunohistochemistry—Mice were transcardially perfused with 4% paraformaldehyde at defined end points. The spinal cord was carefully dissected and post-fixed in 4% paraformaldehyde overnight and then transferred to 30% sucrose in 0.1 M PBS. The tissue was embedded in optimum cutting temperature (OCT) compound (Tissue-Tek), frozen and sectioned using a cryostat (CM3050 S, Leica) at 60 μm. Sections were subsequently warmed at 37 °C for 30 m in and OCT was washed away with PBS. A solution containing 10% normal goat serum (NGS), 0.2% Triton X-100 in PBS was used for blocking at room temperature for 1 h. Sections were then incubated with primary antibodies at 4 °C overnight. After washing three times with PBS, cryosections were incubated with the appropriate Alexa Fluor conjugated secondary antibodies (1:500, Invitrogen). When necessary, sections were counterstained with 4′,6-diamidino-2-phenylindole (DAPI, 1:10000, Thermo Fisher, D1306). The following primary antibody was used: rabbit anti-GFAP (1:1000, Dako, #Z0334). Images were taken using a LSM700 confocal or AxioVision inverted fluorescence microscope (Zeiss).

Protein extraction and immunoblotting—L4–5 DRGs from adult rats or mice were dissected, rinsed shortly in ice-cold HBSS and snap frozen in liquid nitrogen. The samples were mechanically ground with a micropistille in liquid nitrogen and the procedure repeated until the DRGs were powdery. The samples were then lysed on ice in radioimmunoprecipitation assay (RIPA) buffer (50 mM Tris-HCl pH 8.0, 150 mM NaCl, 1% Triton X-100, 0.25% sodium deoxycholate, 0.1% sodium dodecyl sulfate) containing phosphatase (PhosSTOP, Roche, 04906845001) and protease inhibitors (cOmplete, Roche, 11836170001), centrifuged and the supernatant collected. The protein concentration of the lysate was determined using the Precision Red protein assay (Cytoskeleton, Inc.). Total lysates (15–20 μg) were fractionated by 10–12% SDS-polyacrylamide gel electrophoresis (PAGE) and then transferred to a polyvinylidene difluoride (PVDF) membrane (Millipore, ISEQ00010). The membranes were stained with Ponceau S (Applichem, A2935,0500) to confirm equal loading and transfer of the samples. After blocking with 5% nonfat dry milk in TBS-T or 5% BSA in TBS-T at RT for 1 h, membranes were then probed with the appropriate primary antibodies at 4 °C overnigh t, washed 3 times in TBS-T and then incubated with horseradish peroxidase conjugated secondary antibodies (1:20000, GE Healthcare, NA931 or NA934) for 1 h. For protein detection, the membrane was incubated with enhanced chemiluminescence (Pierce™ ECL, Thermo Fisher, 32106) solution. Custom-made primary antibodies have been previously described (Gurniak et al., 2014) and were used as follows: rabbit anti-Cofilin1 (1:2000, KG60), rabbit anti-Cofilin2 (1:2000, FHU1) and mouse monoclonal anti-ADF (1:5, raw supernatant from hybridoma, 7D10). The following commercial primary antibodies were used: rabbit anti-phospho Cofilin1/2, which does not detect phospho-ADF (1:1500, Cell Signaling Technology, #3313), rabbit anti-SSH1L (1:500, ECM Biosciences, SP1711), rabbit anti-phospho SSH1L (1:500, ECM Biosciences, SP3901), mouse anti-LIMK1 (1:250, BD Biosciences, 611748), rabbit anti-phospho LIMK1/2 [pYpT507/508] (1:400, Thermo Fisher, 44–1076G). Rabbit anti-Tuj1 (1:10000, Sigma, T2200) antibody was used as protein loading control.

QUANTIFICATION AND STATISTICAL ANALYSIS

Statistical analysis was performed using one-way ANOVA analysis of variance, followed by Bonferroni post test, or using unpaired Student's *t*-test, as indicated in the figure captions. Statistical analysis of axon regeneration *in vivo* was performed by permutation test, as previously described (Tedeschi et al., 2016).

DATA AND CODE AVAILABILITY

The datasets supporting the current study have not been deposited in a public repository. The reported data is archived on file servers at the German Center for Neurodegenerative Diseases (DZNE), and are available from the corresponding author on request.

Permutation tests were performed using a custom script "permutation_test 0.18" implemented in Python (2.7.3 version) including Pandas and NumPy libraries. The script is available for download in the Python Package Index (https://pypi.python.org/pypi/permutation_test).

KEY RESOURCES TABLE

See the Key Resources Table file.

Supplementary Material

Refer to Web version on PubMed Central for supplementary material.

ACKNOWLEDGMENTS

We thank Gaia Tavosanis, Kelly Kawabata, and Roland Wedlich-Söldner for critically reading and discussing the manuscript. We are grateful for the technical assistance of Jessica Gonyer, Liane Meyn, and Kerstin Weisheit. We would also like to thank the animal facility of the DZNE Bonn. We also extend gratitude to all the members of the F.B. laboratory for productive discussions related to this project. This work was supported by IRP, WfL and DFG (F.B.), as well as by SFB 1089 and SPP 1464 (W.W). A.T. is supported by the Craig H. Neilsen Foundation, the Marina Romoli Onlus Association, the Discovery Themes Initiative on Chronic Brain Injury and the National Institute of Neurological Disorders (R01NS110681). F.B. is a member of the excellence cluster ImmunoSensation2, the SFBs 1089, 1158 and is a recipient of the Leibniz-Prize and of the Roger De Spoelberch Prize.

REFERENCES

Arber S, Barbayannis FA, Hanser H, Schneider C, Stanyon CA, Bernard O, and Caroni P (1998). Regulation of actin dynamics through phosphorylation of cofilin by LIM-kinase. Nature 393, 805–809. [PubMed: 9655397]

Augustine RC, Vidali L, Kleinman KP, and Bezanilla M (2008). Actin depolymerizing factor is essential for viability in plants, and its phosphoregulation is important for tip growth. Plant J 54, 863–875. [PubMed: 18298672]

Bamburg JR, and Bernstein BW (2010). Roles of ADF/cofilin in actin polymerization and beyond. F1000 Biol Rep 2, 62. [PubMed: 21173851]

Bamburg JR, and Bray D (1987). Distribution and cellular localization of actin depolymerizing factor. J Cell Biol 105, 2817–2825. [PubMed: 3320057]

Bamburg JR, and Wiggan OP (2002). ADF/cofilin and actin dynamics in disease. Trends Cell Biol 12, 598–605. [PubMed: 12495849]

Bellenchi GC, Gurniak CB, Perlas E, Middei S, Ammassari-Teule M, and Witke W (2007). N-cofilin is associated with neuronal migration disorders and cell cycle control in the cerebral cortex. Genes Dev 21, 2347–2357. [PubMed: 17875668]

Blanquie O, and Bradke F (2018). Cytoskeleton dynamics in axon regeneration. Curr Opin Neurobiol 51, 60–69. [PubMed: 29544200]

Bradke F, and Dotti CG (1999). The role of local actin instability in axon formation. Science 283, 1931–1934. [PubMed: 10082468]

Bradke F, and Dotti CG (2000). Differentiated neurons retain the capacity to generate axons from dendrites. Curr Biol 10, 1467–1470. [PubMed: 11102812]

Bradke F, Fawcett JW, and Spira ME (2012). Assembly of a new growth cone after axotomy: the precursor to axon regeneration. Nat Rev Neurosci 13, 183–193. [PubMed: 22334213]

Bravo-Cordero JJ, Magalhaes MA, Eddy RJ, Hodgson L, and Condeelis J (2013). Functions of cofilin in cell locomotion and invasion. Nat Rev Mol Cell Biol 14, 405–415. [PubMed: 23778968]

Brieher W (2013). Mechanisms of actin disassembly. Mol Biol Cell 24, 2299–2302. [PubMed: 23900650]

Chandran V, Coppola G, Nawabi H, Omura T, Versano R, Huebner EA, Zhang A, Costigan M, Yekkirala A, Barrett L, et al. (2016). A Systems-Level Analysis of the Peripheral Nerve Intrinsic Axonal Growth Program. Neuron 89, 956–970. [PubMed: 26898779]

Chen H, Bernstein BW, and Bamburg JR (2000). Regulating actin-filament dynamics in vivo. Trends Biochem Sci 25, 19–23. [PubMed: 10637608]

Cho Y, Shin JE, Ewan EE, Oh YM, Pita-Thomas W, and Cavalli V (2015). Activating Injury-Responsive Genes with Hypoxia Enhances Axon Regeneration through Neuronal HIF-1alpha. Neuron 88, 720–734. [PubMed: 26526390]

Cho Y, Sloutsky R, Naegle KM, and Cavalli V (2013). Injury-induced HDAC5 nuclear export is essential for axon regeneration. Cell 155, 894–908. [PubMed: 24209626]

Coles CH, and Bradke F (2015). Coordinating neuronal actin-microtubule dynamics. Curr Biol 25, R677–691. [PubMed: 26241148]

Conde C, Arias C, Robin M, Li A, Saito M, Chuang JZ, Nairn AC, Sung CH, and Caceres A (2010). Evidence for the involvement of Lfc and Tctex-1 in axon formation. J Neurosci 30, 6793–6800. [PubMed: 20463241]

Costigan M, Befort K, Karchewski L, Griffin RS, D'Urso D, Allchorne A, Sitarski J, Mannion JW, Pratt RE, and Woolf CJ (2002). Replicate high-density rat genome oligonucleotide microarrays reveal hundreds of regulated genes in the dorsal root ganglion after peripheral nerve injury. BMC Neurosci 3, 16. [PubMed: 12401135]

Curcio M, and Bradke F (2018). Axon Regeneration in the Central Nervous System: Facing the Challenges from the Inside. Annual review of cell and developmental biology 34, 495–521.

Dawe HR, Minamide LS, Bamburg JR, and Cramer LP (2003). ADF/cofilin controls cell polarity during fibroblast migration. Curr Biol 13, 252–257. [PubMed: 12573223]

Dent EW, Gupton SL, and Gertler FB (2011). The growth cone cytoskeleton in axon outgrowth and guidance. Cold Spring Harb Perspect Biol 3.

Dotti CG, Sullivan CA, and Banker GA (1988). The establishment of polarity by hippocampal neurons in culture. J Neurosci 8, 1454–1468. [PubMed: 3282038]

Eiseler T, Doppler H, Yan IK, Kitatani K, Mizuno K, and Storz P (2009). Protein kinase D1 regulates cofilin-mediated F-actin reorganization and cell motility through slingshot. Nat Cell Biol 11, 545–556. [PubMed: 19329994]

Endo M, Ohashi K, and Mizuno K (2007). LIM kinase and slingshot are critical for neurite extension. J Biol Chem 282, 13692–13702. [PubMed: 17360713]

Endo M, Ohashi K, Sasaki Y, Goshima Y, Niwa R, Uemura T, and Mizuno K (2003). Control of growth cone motility and morphology by LIM kinase and Slingshot via phosphorylation and dephosphorylation of cofilin. J Neurosci 23, 2527–2537. [PubMed: 12684437]

Fawcett JW (2015). The extracellular matrix in plasticity and regeneration after CNS injury and neurodegenerative disease. Prog Brain Res 218, 213–226. [PubMed: 25890139]

Feng G, Mellor RH, Bernstein M, Keller-Peck C, Nguyen QT, Wallace M, Nerbonne JM, Lichtman JW, and Sanes JR (2000). Imaging neuronal subsets in transgenic mice expressing multiple spectral variants of GFP. Neuron 28, 41–51. [PubMed: 11086982]

Flynn KC, Hellal F, Neukirchen D, Jacob S, Tahirovic S, Dupraz S, Stern S, Garvalov BK, Gurniak C, Shaw AE, et al. (2012). ADF/cofilin-mediated actin retrograde flow directs neurite formation in the developing brain. Neuron 76, 1091–1107. [PubMed: 23259946]

Forscher P, and Smith SJ (1988). Actions of cytochalasins on the organization of actin filaments and microtubules in a neuronal growth cone. J Cell Biol 107, 1505–1516. [PubMed: 3170637]

Garvalov BK, Flynn KC, Neukirchen D, Meyn L, Teusch N, Wu X, Brakebusch C, Bamburg JR, and Bradke F (2007). Cdc42 regulates cofilin during the establishment of neuronal polarity. J Neurosci 27, 13117–13129. [PubMed: 18045906]

Gomis-Ruth S, Wierenga CJ, and Bradke F (2008). Plasticity of polarization: changing dendrites into axons in neurons integrated in neuronal circuits. Curr Biol 18, 992–1000. [PubMed: 18595703]

Gurniak CB, Chevessier F, Jokwitz M, Jonsson F, Perlas E, Richter H, Matern G, Boyl PP, Chaponnier C, Furst D, et al. (2014). Severe protein aggregate myopathy in a knockout mouse model points to an essential role of cofilin2 in sarcomeric actin exchange and muscle maintenance. Eur J Cell Biol 93, 252–266. [PubMed: 24598388]

Gurniak CB, Perlas E, and Witke W (2005). The actin depolymerizing factor n-cofilin is essential for neural tube morphogenesis and neural crest cell migration. Dev Biol 278, 231–241. [PubMed: 15649475]

He Z, and Jin Y (2016). Intrinsic Control of Axon Regeneration. Neuron 90, 437–451. [PubMed: 27151637]

Hellal F, Hurtado A, Ruschel J, Flynn KC, Laskowski CJ, Umlauf M, Kapitein LC, Strikis D, Lemmon V, Bixby J, et al. (2011). Microtubule stabilization reduces scarring and causes axon regeneration after spinal cord injury. Science 331, 928–931. [PubMed: 21273450]

Hilton BJ, Blanquie O, Tedeschi A, and Bradke F (2019). High-resolution 3D imaging and analysis of axon regeneration in unsectioned spinal cord with or without tissue clearing. Nat Protoc 14, 1235–1260. [PubMed: 30903109]

Hilton BJ, and Bradke F (2017). Can injured adult CNS axons regenerate by recapitulating development? Development 144, 3417–3429. [PubMed: 28974639]

Hu G, Huang K, Hu Y, Du G, Xue Z, Zhu X, and Fan G (2016). Single-cell RNA-seq reveals distinct injury responses in different types of DRG sensory neurons. Sci Rep 6, 31851. [PubMed: 27558660]

Kaplan A, Morquette B, Kroner A, Leong S, Madwar C, Sanz R, Banerjee SL, Antel J, Bisson N, David S, et al. (2017). Small-Molecule Stabilization of 14–3-3 Protein-Protein Interactions Stimulates Axon Regeneration. Neuron 93, 1082–1093 e1085. [PubMed: 28279353]

Kremneva E, Makkonen MH, Skwarek-Maruszewska A, Gateva G, Michelot A, Dominguez R, and Lappalainen P (2014). Cofilin-2 controls actin filament length in muscle sarcomeres. Dev Cell 31, 215–226. [PubMed: 25373779]

Kuhn TB, Meberg PJ, Brown MD, Bernstein BW, Minamide LS, Jensen JR, Okada K, Soda EA, and Bamburg JR (2000). Regulating actin dynamics in neuronal growth cones by ADF/cofilin and rho family GTPases. J Neurobiol 44, 126–144. [PubMed: 10934317]

Kunda P, Paglini G, Quiroga S, Kosik K, and Caceres A (2001). Evidence for the involvement of Tiam1 in axon formation. J Neurosci 21, 2361–2372. [PubMed: 11264310]

Lowery LA, and Van Vactor D (2009). The trip of the tip: understanding the growth cone machinery. Nat Rev Mol Cell Biol 10, 332–343. [PubMed: 19373241]

McQuarrie IG, Grafstein B, and Gershon MD (1977). Axonal regeneration in the rat sciatic nerve: effect of a conditioning lesion and of dbcAMP. Brain Res 132, 443–453. [PubMed: 199316]

Meberg PJ (2000). Signal-regulated ADF/cofilin activity and growth cone motility. Mol Neurobiol 21, 97–107. [PubMed: 11327152]

Meberg PJ, Ono S, Minamide LS, Takahashi M, and Bamburg JR (1998). Actin depolymerizing factor and cofilin phosphorylation dynamics: response to signals that regulate neurite extension. Cell Motil Cytoskeleton 39, 172–190. [PubMed: 9484959]

Mizuno K (2013). Signaling mechanisms and functional roles of cofilin phosphorylation and dephosphorylation. Cell Signal 25, 457–469. [PubMed: 23153585]

Moriyama K, Iida K, and Yahara I (1996). Phosphorylation of Ser-3 of cofilin regulates its essential function on actin. Genes to cells : devoted to molecular & cellular mechanisms 1, 73–86. [PubMed: 9078368]

Moriyama K, and Yahara I (1999). Two activities of cofilin, severing and accelerating directional depolymerization of actin filaments, are affected differentially by mutations around the actin-binding helix. EMBO J 18, 6752–6761. [PubMed: 10581248]

Moriyama K, and Yahara I (2002). The actin-severing activity of cofilin is exerted by the interplay of three distinct sites on cofilin and essential for cell viability. Biochem J 365, 147–155. [PubMed: 12113256]

Neumann S, Bradke F, Tessier-Lavigne M, and Basbaum AI (2002). Regeneration of sensory axons within the injured spinal cord induced by intraganglionic cAMP elevation. Neuron 34, 885–893. [PubMed: 12086637]

Neumann S, and Woolf CJ (1999). Regeneration of dorsal column fibers into and beyond the lesion site following adult spinal cord injury. Neuron 23, 83–91. [PubMed: 10402195]

Nishita M, Wang Y, Tomizawa C, Suzuki A, Niwa R, Uemura T, and Mizuno K (2004). Phosphoinositide 3-kinase-mediated activation of cofilin phosphatase Slingshot and its role for insulin-induced membrane protrusion. J Biol Chem 279, 7193–7198. [PubMed: 14645219]

O'Connor TP, and Bentley D (1993). Accumulation of actin in subsets of pioneer growth cone filopodia in response to neural and epithelial guidance cues in situ. J Cell Biol 123, 935–948. [PubMed: 8227150]

Oh YM, Mahar M, Ewan EE, Leahy KM, Zhao G, and Cavalli V (2018). Epigenetic regulator UHRF1 inactivates REST and growth suppressor gene expression via DNA methylation to promote axon regeneration. Proc Natl Acad Sci U S A 115, E12417–E12426. [PubMed: 30530687]

Oleinik NV, Krupenko NI, and Krupenko SA (2010). ALDH1L1 inhibits cell motility via dephosphorylation of cofilin by PP1 and PP2A. Oncogene 29, 6233–6244. [PubMed: 20729910]

Ono S (2007). Mechanism of depolymerization and severing of actin filaments and its significance in cytoskeletal dynamics. Int Rev Cytol 258, 1–82. [PubMed: 17338919]

Pak CW, Flynn KC, and Bamburg JR (2008). Actin-binding proteins take the reins in growth cones. Nat Rev Neurosci 9, 136–147. [PubMed: 18209731]

Pollard TD, Blanchoin L, and Mullins RD (2000). Molecular mechanisms controlling actin filament dynamics in nonmuscle cells. Annu Rev Biophys Biomol Struct 29, 545–576. [PubMed: 10940259]

Puttagunta R, Tedeschi A, Soria MG, Hervera A, Lindner R, Rathore KI, Gaub P, Joshi Y, Nguyen T, Schmandke A, et al. (2014). PCAF-dependent epigenetic changes promote axonal regeneration in the central nervous system. Nat Commun 5, 3527. [PubMed: 24686445]

Qiu J, Cai D, Dai H, McAtee M, Hoffman PN, Bregman BS, and Filbin MT (2002). Spinal axon regeneration induced by elevation of cyclic AMP. Neuron 34, 895–903. [PubMed: 12086638]

Richardson PM, and Issa VM (1984). Peripheral injury enhances central regeneration of primary sensory neurones. Nature 309, 791–793. [PubMed: 6204205]

Riedl J, Crevenna AH, Kessenbrock K, Yu JH, Neukirchen D, Bista M, Bradke F, Jenne D, Holak TA, Werb Z, et al. (2008). Lifeact: a versatile marker to visualize F-actin. Nat Methods 5, 605–607. [PubMed: 18536722]

Rodriguez OC, Schaefer AW, Mandato CA, Forscher P, Bement WM, and Waterman-Storer CM (2003). Conserved microtubule-actin interactions in cell movement and morphogenesis. Nat Cell Biol 5, 599–609. [PubMed: 12833063]

Rosenblatt J, Agnew BJ, Abe H, Bamburg JR, and Mitchison TJ (1997). Xenopus actin depolymerizing factor/cofilin (XAC) is responsible for the turnover of actin filaments in Listeria monocytogenes tails. J Cell Biol 136, 1323–1332. [PubMed: 9087446]

Ruschel J, and Bradke F (2017). Systemic administration of epothilone D improves functional recovery of walking after rat spinal cord contusion injury. Exp Neurol.

Ruschel J, Hellal F, Flynn KC, Dupraz S, Elliott DA, Tedeschi A, Bates M, Sliwinski C, Brook G, Dobrindt K, et al. (2015). Axonal regeneration. Systemic administration of epothilone B promotes axon regeneration after spinal cord injury. Science 348, 347–352. [PubMed: 25765066]

Sandner B, Puttagunta R, Motsch M, Bradke F, Ruschel J, Blesch A, and Weidner N (2018). Systemic epothilone D improves hindlimb function after spinal cord contusion injury in rats. Exp Neurol.

Schaffran B, Hilton BJ, and Bradke F (2019). Imaging in vivo dynamics of sensory axon responses to CNS injury. Exp Neurol 317, 110–118. [PubMed: 30794766]

Schwab ME, and Strittmatter SM (2014). Nogo limits neural plasticity and recovery from injury. Curr Opin Neurobiol 27, 53–60. [PubMed: 24632308]

Silver DJ, and Silver J (2014). Contributions of chondroitin sulfate proteoglycans to neurodevelopment, injury, and cancer. Curr Opin Neurobiol 27, 171–178. [PubMed: 24762654]

Sivadasan R, Hornburg D, Drepper C, Frank N, Jablonka S, Hansel A, Lojewski X, Sterneckert J, Hermann A, Shaw PJ, et al. (2016). C9ORF72 interaction with cofilin modulates actin dynamics in motor neurons. Nat Neurosci 19, 1610–1618. [PubMed: 27723745]

Smith DS, and Skene JH (1997). A transcription-dependent switch controls competence of adult neurons for distinct modes of axon growth. J Neurosci 17, 646–658. [PubMed: 8987787]

Sun F, Park KK, Belin S, Wang D, Lu T, Chen G, Zhang K, Yeung C, Feng G, Yankner BA, et al. (2011). Sustained axon regeneration induced by co-deletion of PTEN and SOCS3. Nature 480, 372–375. [PubMed: 22056987]

Takano T, Xu C, Funahashi Y, Namba T, and Kaibuchi K (2015). Neuronal polarization. Development 142, 2088–2093. [PubMed: 26081570]

Tedeschi A (2011). Tuning the orchestra: transcriptional pathways controlling axon regeneration. Front Mol Neurosci 4, 60. [PubMed: 22294979]

Tedeschi A, and Bradke F (2017). Spatial and temporal arrangement of neuronal intrinsic and extrinsic mechanisms controlling axon regeneration. Curr Opin Neurobiol 42, 118–127. [PubMed: 28039763]

Tedeschi A, Dupraz S, Laskowski CJ, Xue J, Ulas T, Beyer M, Schultze JL, and Bradke F (2016). The Calcium Channel Subunit Alpha2delta2 Suppresses Axon Regeneration in the Adult CNS. Neuron 92, 419–434. [PubMed: 27720483]

van Beuningen SFB, Will L, Harterink M, Chazeau A, van Battum EY, Frias CP, Franker MAM, Katrukha EA, Stucchi R, Vocking K, et al. (2015). TRIM46 Controls Neuronal Polarity and Axon Specification by Driving the Formation of Parallel Microtubule Arrays. Neuron 88, 1208–1226. [PubMed: 26671463]

Van Goor D, Hyland C, Schaefer AW, and Forscher P (2012). The role of actin turnover in retrograde actin network flow in neuronal growth cones. PLoS One 7, e30959. [PubMed: 22359556]

Vartiainen MK, Mustonen T, Mattila PK, Ojala PJ, Thesleff I, Partanen J, and Lappalainen P (2002). The three mouse actin-depolymerizing factor/cofilins evolved to fulfill cell-type-specific requirements for actin dynamics. Mol Biol Cell 13, 183–194. [PubMed: 11809832]

Wang Y, Shibasaki F, and Mizuno K (2005). Calcium signal-induced cofilin dephosphorylation is mediated by Slingshot via calcineurin. J Biol Chem 280, 12683–12689. [PubMed: 15671020]

Weng YL, Wang X, An R, Cassin J, Vissers C, Liu Y, Liu Y, Xu T, Wang X, Wong SZH, et al. (2018). Epitranscriptomic m(6)A Regulation of Axon Regeneration in the Adult Mammalian Nervous System. Neuron 97, 313–325 e316. [PubMed: 29346752]

Witte H, Neukirchen D, and Bradke F (2008). Microtubule stabilization specifies initial neuronal polarization. J Cell Biol 180, 619–632. [PubMed: 18268107]

Ylera B, Erturk A, Hellal F, Nadrigny F, Hurtado A, Tahirovic S, Oudega M, Kirchhoff F, and Bradke F (2009). Chronically CNS-injured adult sensory neurons gain regenerative competence upon a lesion of their peripheral axon. Curr Biol 19, 930–936. [PubMed: 19409789]

Yogev S, and Shen K (2017). Establishing Neuronal Polarity with Environmental and Intrinsic Mechanisms. Neuron 96, 638–650. [PubMed: 29096077]

HIGHLIGHTS

1. Elevated actin turnover is essential for regenerative growth
2. ADF/Cofilin activity increases during conditioning-mediated regeneration
3. ADF/Cofilin is necessary and sufficient for axon regeneration
4. The severing activity of ADF/Cofilin is critical for axon regeneration

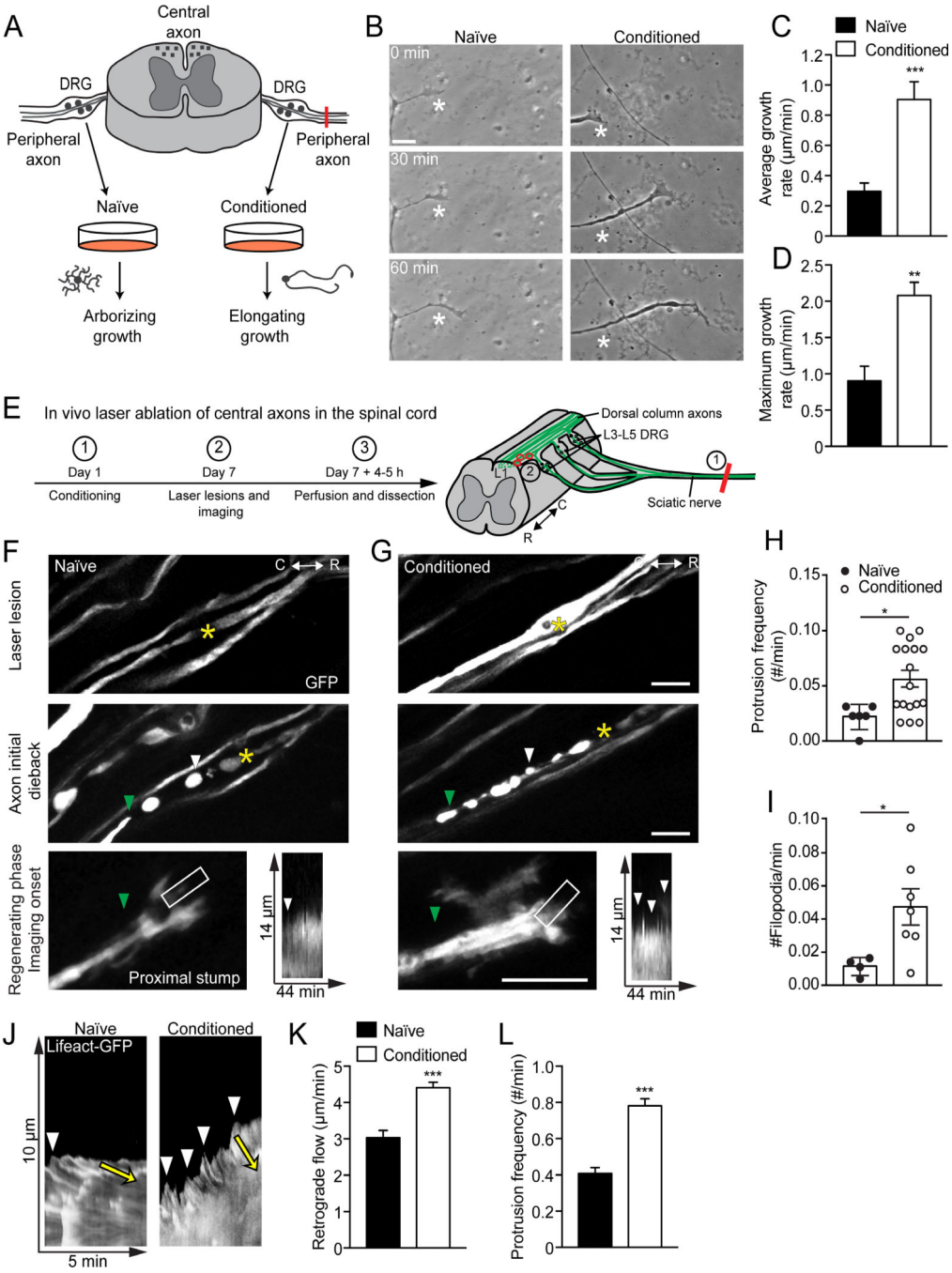

Figure 1. Actin Dynamics are Required for Fast Axonal Growth Induced by Conditioning Lesion

(A) Scheme of the conditioning effect.

(B) Live-cell imaging of naïve and conditioned rat DRG neurons 15–16 h after plating. Asterisks indicate stable landmarks. Scale bar, 10 µm.

(C and D) Average and maximum growth rate of (B). Values are plotted as mean and SEM (**p < 0.01, ***p < 0.001 by Student's *t* test. (C) n = 13 to 15 neurons;

(D) n = 5 neurons from three independent experiments.

(E) Timeline of *in vivo* laser ablation of axons.

(F and G) *In vivo* imaging after laser-induced lesion in naïve (F) and conditioned (G) DRG axons in the spinal cord of GFP-M mice. Kymographs represent the protrusion dynamics in the analyzed area (white box). Green and white arrowheads indicate the proximal axon stump and axon dieback respectively. Scale bar, 20 μm.

(H) Protrusion frequency in growth cones of naïve and conditioned DRG axons observed in kymographs from 30 min to 1 h-long movies. Values are plotted as mean and SEM (*$p<0.05$ by Student's *t* test. n = 6 to 17 axons from 8 different mice).

(I) Filopodia frequency up to 4.5 hours after lesion. Values are plotted as mean and SEM (*$p<0.05$ by Student's *t* test. n = 4 to 12 axons from 8 different mice).

(J) Kymographs from live-cell imaging of naïve and conditioned rat DRG neurons expressing Lifeact-GFP. Yellow arrows indicate actin translocation and white arrowheads highlight sites of actin protrusion.

(K and L) Actin retrograde flow (K) and protrusion frequency (L) of (F and G). Values are plotted as mean and SEM (***$p < 0.001$ by Student's *t* test. n = 36 to 49 neurons from three independent experiments).

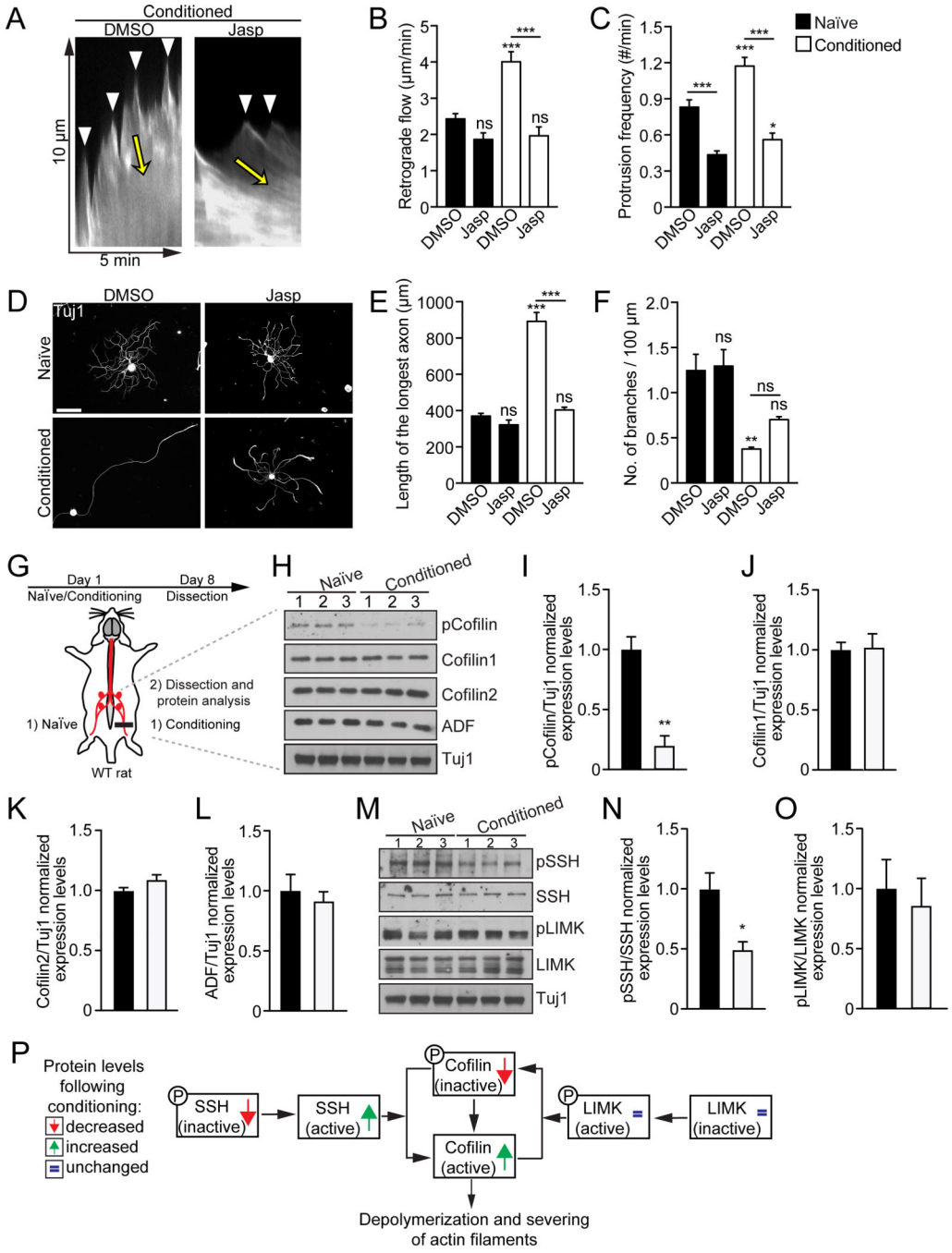

Figure 2. ADF/Cofilin Activity Increases Following a Conditioning Lesion

(A) Kymographs from live-cell imaging of conditioned rat DRG neurons expressing Lifeact-GFP with indicated treatments. Yellow arrows highlight actin translocation and white arrowheads sites of actin protrusion.

(B and C) Actin retrograde flow and protrusion frequency of (A). Values are plotted as mean and SEM (*p < 0.05, ***p < 0.001; ns, not significant by one-way ANOVA followed by Bonferroni post test. n = 38 to 57 neurons from four independent experiments).

(D) Beta-3 tubulin (Tuj1) immunolabeling of naïve and conditioned rat DRG neurons cultured for 15–16 h with the indicated treatments. Scale bar, 100 μm.
(E and F) Maximal axon length and branching frequency of (D). Values are plotted as mean and SEM (**p < 0.01, ***p < 0.001; ns, not significant by one-way ANOVA followed by Bonferroni post test. n > 90 neurons from three independent experiments).
(G) Timeline to assess AC protein levels following conditioning lesion.
(H and M) Immunoblots of indicated proteins in rat L4–5 DRG extracts. Tuj1 is shown as loading control (n = 3 animals per group; each line represents an independent animal).
(I, J, K, L) Normalized protein levels shown in (H). Values are plotted as mean and SEM (**p < 0.01 by Student's *t* test).
(N and O) Normalized protein levels shown in (M). Values are plotted as mean and SEM (*p < 0.05 by Student's *t* test).
(P) Signaling pathways regulating Cofilin activity.
Bar color-code for panels B, E, F, J, K, L, N, O follows the legends displayed in panels C and I: black and white refers to naïve and conditioned neurons, respectively. See also Figure S1; Movies S1, S2 and S4.

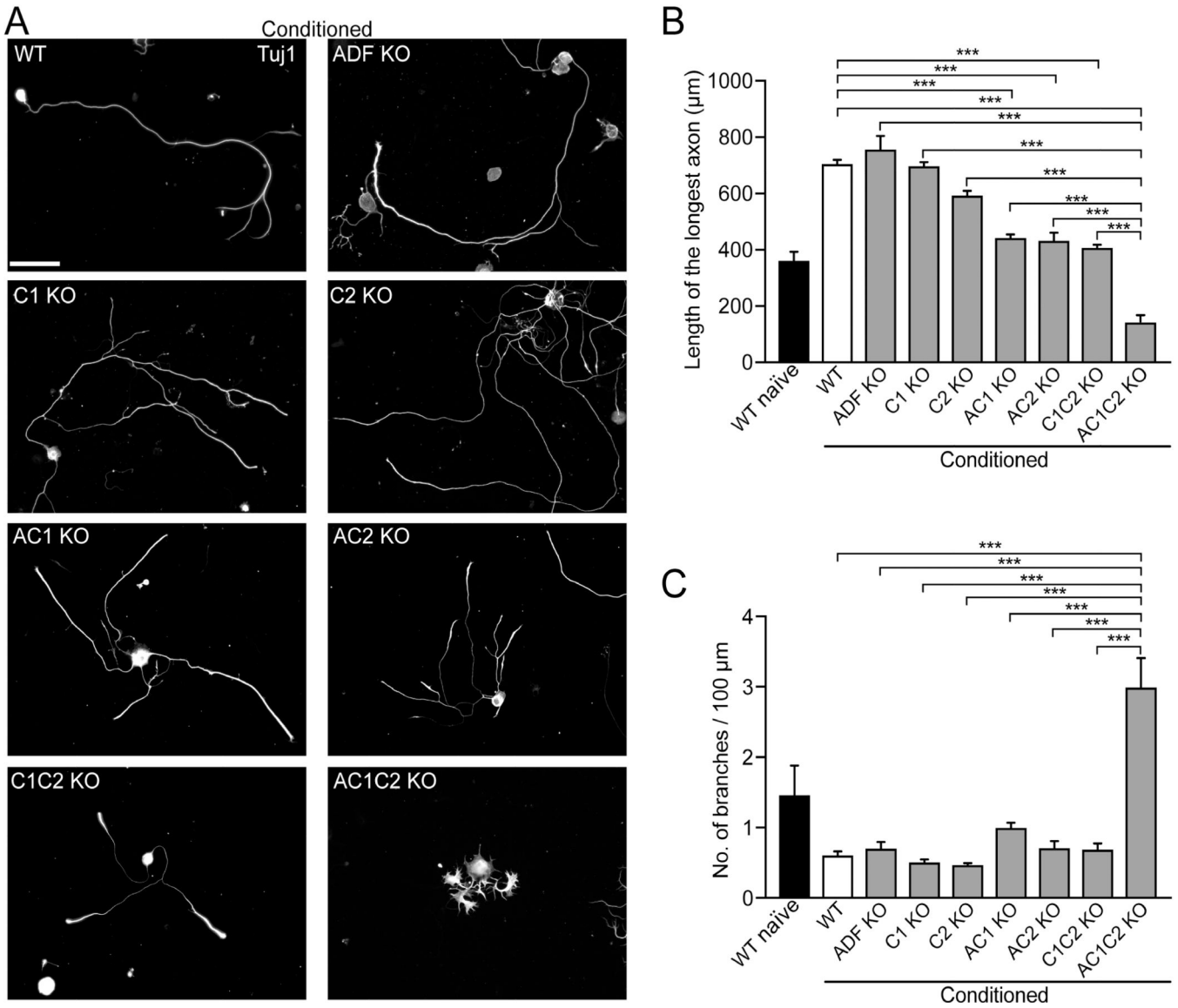

Figure 3. ADF/Cofilin Activity is Required for Axon Elongation

(A) Tuj1 immunolabeling of conditioned dissociated mouse DRG neurons from different mouse lines transduced with AAVs. Scale bar, 100 µm.

(B and C) Maximal axon length and branching frequency of (A). Values are plotted as mean and SEM (***$p < 0.001$ by one-way ANOVA followed by Bonferroni post test. n = 74 to 200 neurons from at least three independent experiments). See also Figures S2 and S3; Movie S5.

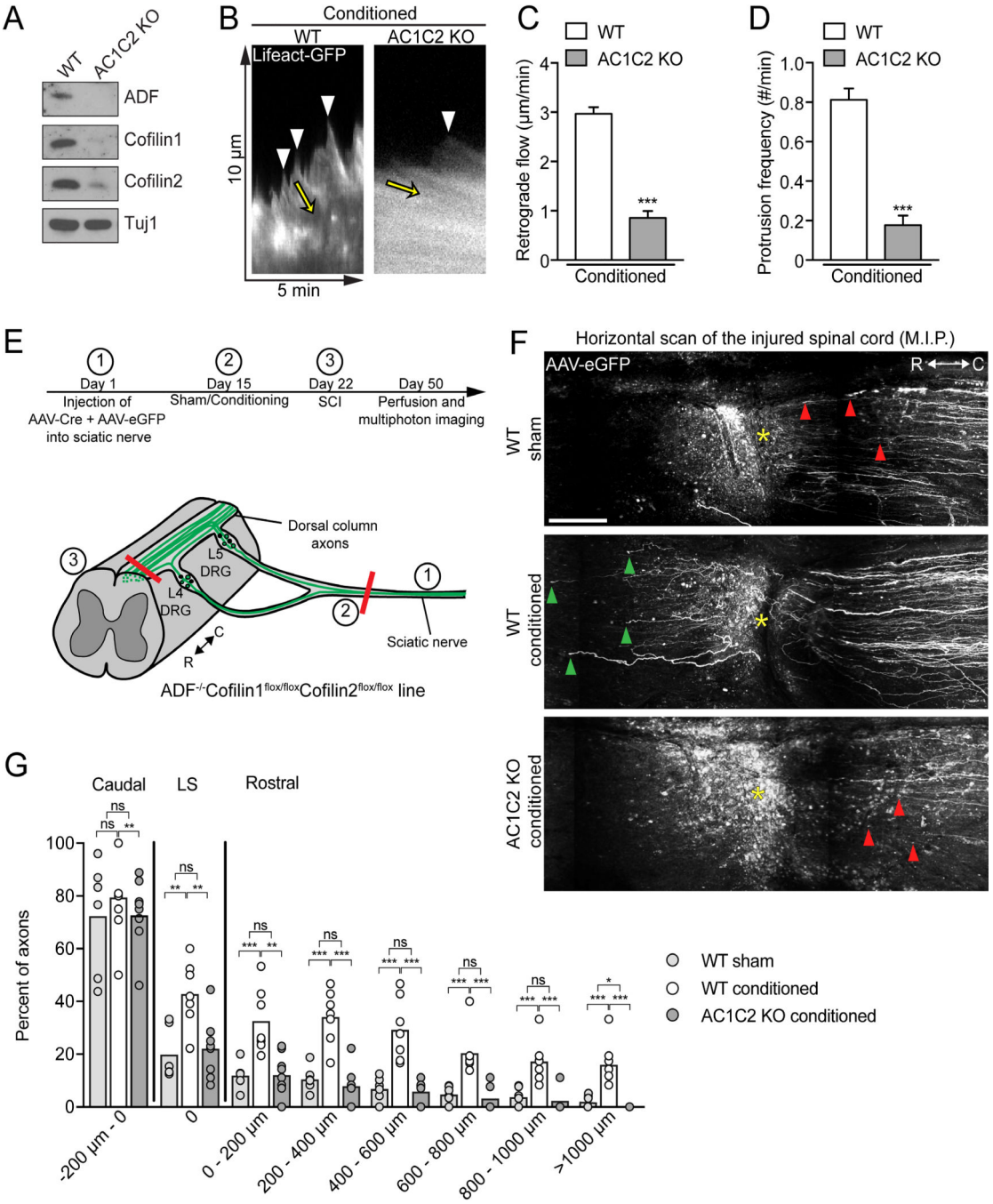

Figure 4. ADF/Cofilin Activity is Required for Actin Dynamics and Axon Regeneration

(A) Immunoblots of AC proteins in WT and AC1C2 KO mouse L4–5 DRG extracts.

(B) Kymographs from live-cell imaging of conditioned WT and AC1C2 KO DRG neurons expressing Lifeact-GFP. Yellow arrows indicate actin translocation and white arrowheads highlight sites of actin protrusion.

(C and D) Actin retrograde flow and protrusion frequency of (B). Values are plotted as mean and SEM (***p < 0.001 by Student's *t* test. n = 25 to 38 neurons from three independent experiments).

(E) Timeline to assess axon regeneration and scheme of the experimental paradigm. SCI, sciatic nerve crush injury; R, rostral; C, caudal.

(F) Automated multiphoton tile scanning of the unsectioned adult spinal cord 4 weeks after SCI. Dorsal column axons were visualized by AAV-eGFP signal. Asterisks indicate the lesion epicenter, arrowheads indicate stalled (red) and regenerating (green) axons. R, rostral; C, caudal. Scale bar, 200 μm.

(G) Quantification of (F). Scatter plot with mean (*$p < 0.05$, **$p < 0.01$, ***$p < 0.001$; ns, not significant by permutation test. n = 6 to 9 animals per group). See also Figure S4 and Movie S6.

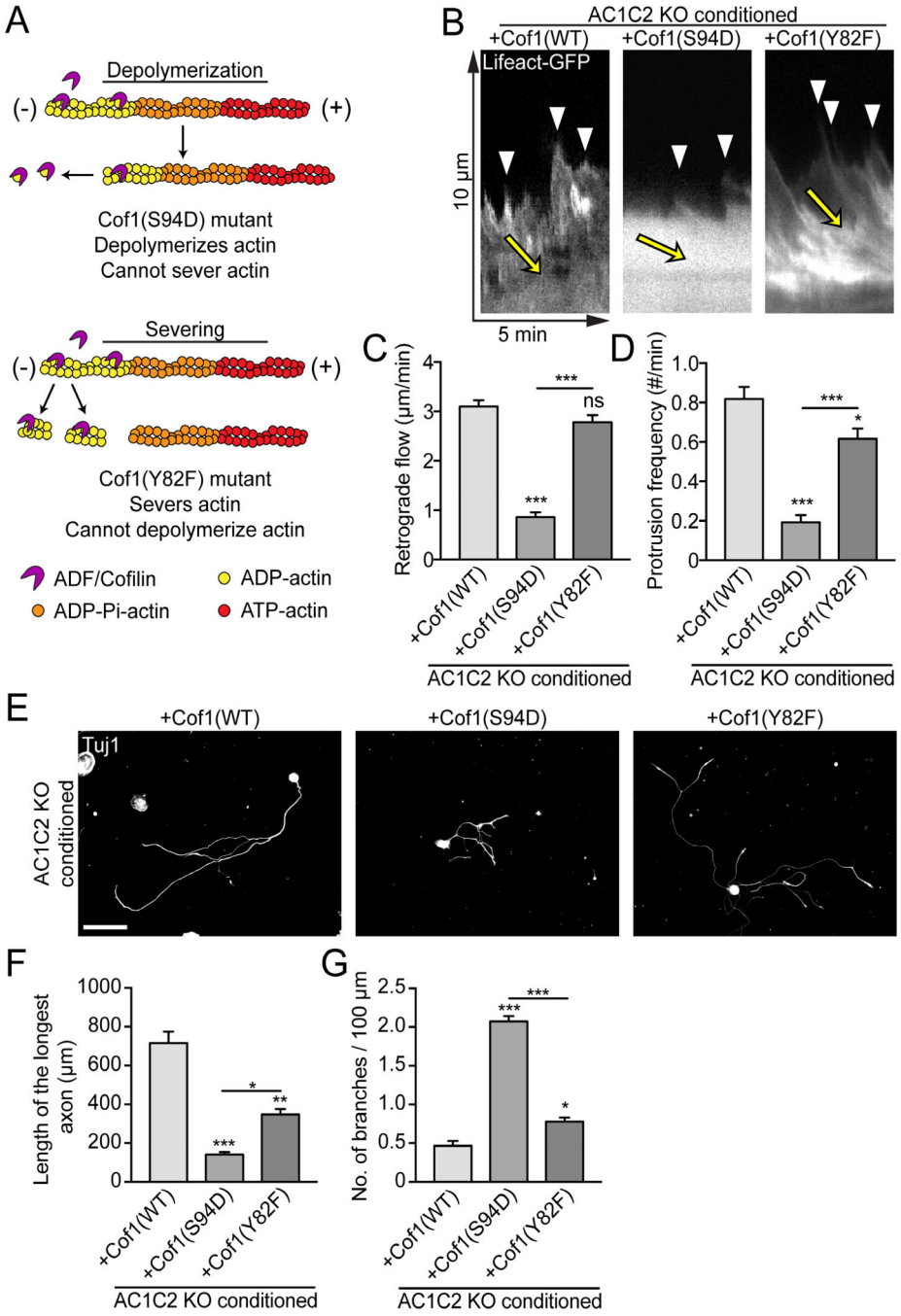

Figure 5. The Severing Activity of Cofilin1 Promotes Actin Turnover and Axon Extension

(A) Scheme of the Cofilin1 mutants.

(B) Kymographs from live-cell imaging of conditioned AC1C2 KO neurons expressing either Cofilin1(WT) or Cofilin1 mutants, as indicated, and Lifeact-GFP. Yellow arrows indicate actin translocation and white arrowheads highlight sites of actin protrusion.

(C and D) Actin retrograde flow and protrusion frequency of (B). Values are plotted as mean and SEM (*p < 0.05, ***p < 0.001; ns, not significant by one-way ANOVA followed by Bonferroni post test. n = 28 to 38 neurons from three independent experiments).

(E) Tuj1 immunolabeling of conditioned dissociated mouse AC1C2 KO DRG neurons expressing either Cofilin1(WT) or Cofilin1 mutants, as indicated. Scale bar, 100 μm.
(F and G) Maximal axon length and branching frequency of (E). Values are plotted as mean and SEM (*$p < 0.05$, **$p < 0.01$, ***$p < 0.001$ by one-way ANOVA followed by Bonferroni post test. n = 93 to 110 neurons from three independent experiments). See also Movie S7.

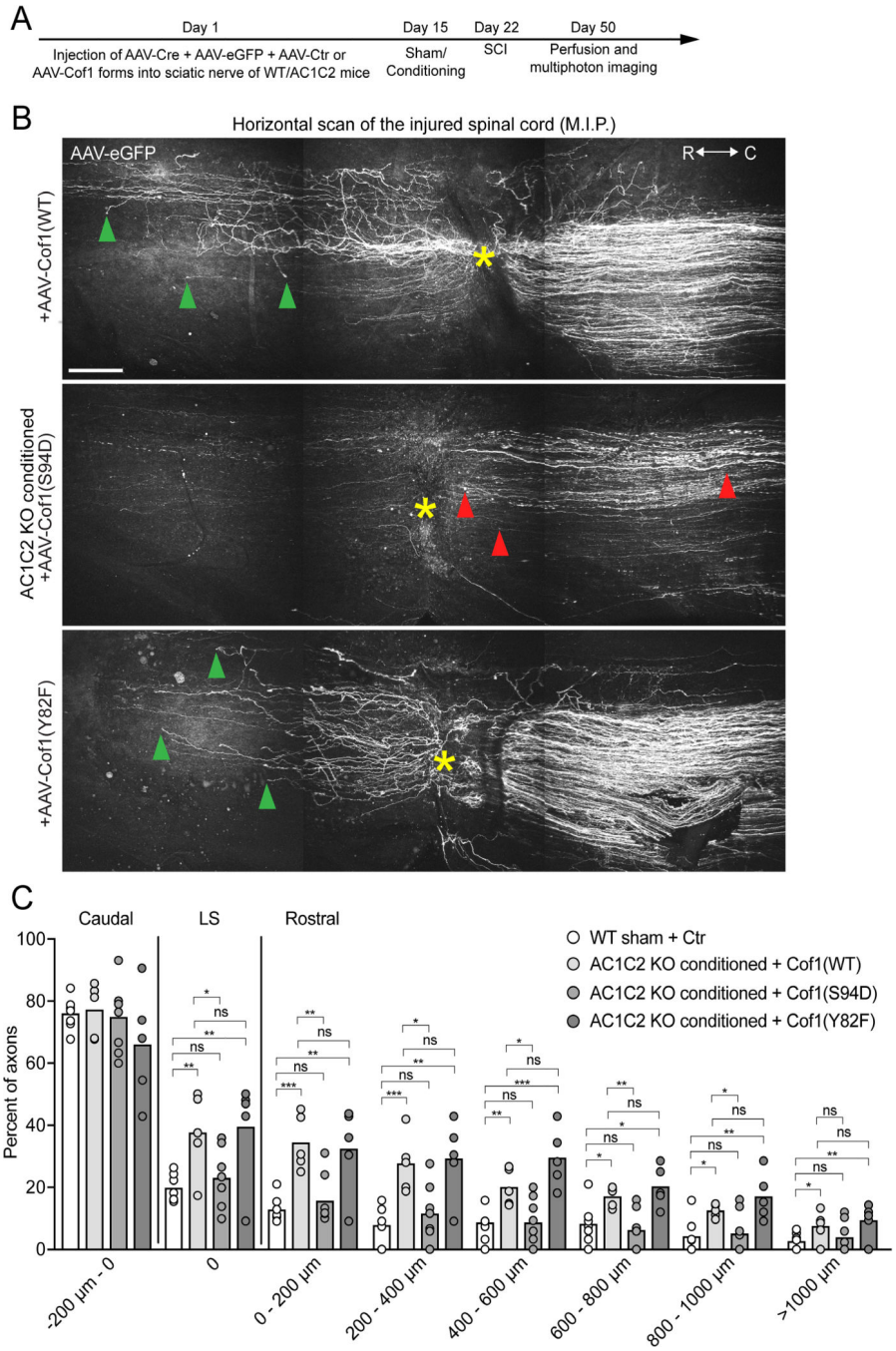

Figure 6. The Severing Activity of Cofilin1 Promotes Axon Regeneration

(A) Timeline to assess axon regeneration.

(B) Automated multiphoton tile scanning of the unsectioned adult spinal cord. Dorsal column axons expressing Cofilin1(WT), Cofilin1(S94D) or Cofilin1(Y82F) were visualized by AAV-eGFP signal. Asterisks indicate the lesion epicenter, arrowheads indicate stalled (red) and regenerating (green) axons. R, rostral; C, caudal. Scale bar, 200 µm.

(C) Quantification of (B). Scatter plot with mean (*p < 0.05, **p < 0.01, ***p < 0.001; ns, not significant by permutation test. n = 5 to 8 animals per group).

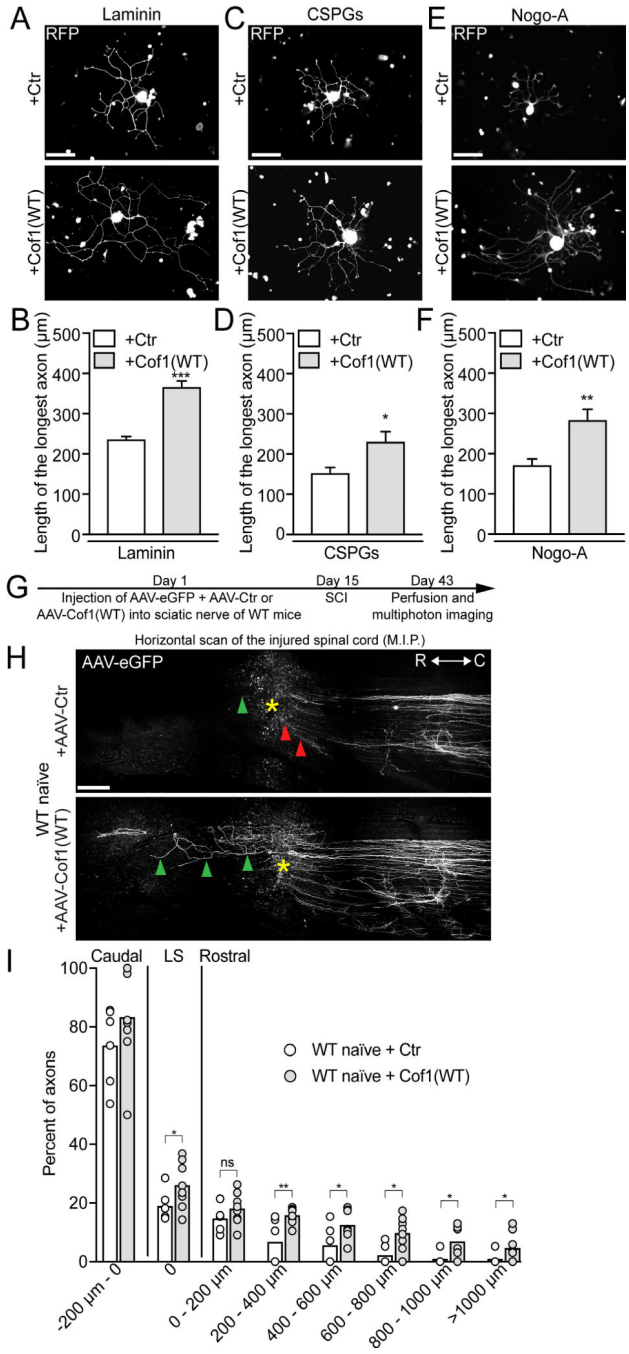

Figure 7. Cofilin1 Drives Axon Extension both *in vitro* and *in vivo*

(A) RFP signal of naïve dissociated rat DRG neurons cultured for 16–18 h on laminin after electroporation with RFP-Control (Ctr), Cofilin1(WT) -expressing plasmids. Scale bar, 100 µm.

(B) Maximal axon length of (A).

(C) RFP signal of naïve dissociated rat DRG neurons cultured for 16–18 h on CSPGs after electroporation with RFP-Control (Ctr) or Cofilin1(WT) -expressing plasmids. Scale bar, 100 µm.

(D) Maximal axon length of (C).
(E) RFP signal of naïve dissociated rat DRG neurons cultured for 16–18 h on Nogo-A after electroporation with eGFP-Control (Ctr) or Cofilin1(WT)-expressing plasmids. Scale bar, 100 μm.
(F) Maximal axon length of (E). Values are plotted as mean and SEM ((B), (D) and (F) *p < 0.05, **p < 0.01, ***p < 0.001; ns, not significant by Student's *t* test. n = 65 to 95 neurons from at least three independent experiments).
(G) Timeline to assess axon regeneration.
(H) Automated multiphoton tile scanning of the unsectioned adult spinal cord. Dorsal column axons expressing AAV-Ctr or AAV-Cofilin1(WT) were visualized by AAV-eGFP signal. Asterisks indicate the lesion epicenter, arrowheads indicate stalled (red) and regenerating (green) axons. R, rostral; C, caudal. Scale bar, 200 μm.
(I) Quantification of (H). Scatter plot with mean (*p < 0.05, **p < 0.01; ns, not significant by permutation test. n = 6 to 8 animals per group).